catalysts

MDPI

Article

Hierarchical Porous Carbon Fibers for Enhanced Interfacial Electron Transfer of Electroactive Biofilm Electrode

Ruijie Wang [1,2], Xiaoshuai Wu [3], Chang Liu [1,2], Jing Yang [1,2], Xian Luo [1,2], Long Zou [4], Zhisong Lu [1,2] and Yan Qiao [1,2,*]

[1] Institute for Clean Energy and Advanced Materials, School of Materials and Energy, Southwest University, Chongqing 400715, China
[2] Chongqing Key Laboratory for Advanced Materials and Technologies of Clean Energies, Chongqing 400715, China
[3] Institute of Materials Science and Devices, Suzhou University of Science and Technology, Suzhou 215011, China
[4] College of Life Sciences, Jiangxi Normal University, Nanchang 330022, China
* Correspondence: yanqiao@swu.edu.cn

Abstract: The nanoporous carbon fiber materials derived from electrospun polyacrylonitrile (PAN) fibers doped with zeolitic imidazolate framework are developed here and applied in the microbe fuel cell anode for enhanced interfacial electron transfer. Zeolitic imidazolate fram-8 (ZIF-8) could introduce a large number of mesopores into fibers, which significantly promote indirect electron transfer mediated by flavins (IET). Moreover, it is noted that thinner fibers are more suitable for cytochromes-based direct electron transfer (DET). Furthermore, the enlarged fiber interspace strengthens the amount of biofilm loading but a larger interspace between thick fibers would hinder the formation of continuous biofilm. Consequently, the nanoporous carbon fiber derived from PAN/ZIF-8 composite with a 1:1 wt ratio shows the best performance according to its suitable mesoporous structure and optimal fiber diameter, which delivers a 10-fold higher maximum power density in microbial fuel cells compared to carbon fabric. In this work, we reveal that the proportion of IET and DET in the interfacial electron transfer process varies with different porous structures and fiber diameters, which may provide some insights for designing porous fiber electrodes for microbial fuel cells and also other devices of bioelectrochemical systems.

Keywords: nanoporous carbon fiber; electroactive biofilm; interfacial electron transfer; hierarchical porous structure

Citation: Wang, R.; Wu, X.; Liu, C.; Yang, J.; Luo, X.; Zou, L.; Lu, Z.; Qiao, Y. Hierarchical Porous Carbon Fibers for Enhanced Interfacial Electron Transfer of Electroactive Biofilm Electrode. *Catalysts* **2022**, *12*, 1187. https://doi.org/10.3390/catal12101187

Academic Editors: Mohd Rafatullah, Yang-Chun Yong and Syed Zaghum Abbas

Received: 7 September 2022
Accepted: 4 October 2022
Published: 7 October 2022

1. Introduction

The interfacial electron transfer process between the solid electrode and the electroactive biofilm is the key step for bioelectrochemical systems (BES) devices such as microbial fuel cells (MFCs) or microbial electrolysis cells (MECs). There are different pathways for interfacial electron transfer such as electron shuttles mediated indirect electron transfer (IET) and outer membrane cytochromes mediated direct electron transfer (DET) [1,2]. The interfacial electron transfer process mainly depends on the ability of the microbes to utilize the extracellular electron acceptors, but the surface structure and properties of the solid electrode also affect it a lot. It has been reported that the mesopores (pore width 2–50 nm) are more favorable for flavin-based IET in *Shewanella* sp. catalyzed MFCs than the micropores (pore width less than 2 nm) [3,4]. The open mesopores with appropriate pore size and pore shape could provide suitable space for the two-electron oxidation of the flavins on the electrode surface. On the other hand, the macroscopic pores which could promote the biofilm adhesion are also critical for both IET and DET. The DET process requires physical contact between the solid electrode and the outer membrane of the bacteria cells so that increased biofilm adhesion could enhance the DET process. At the same time,

biofilm formation could guarantee a high concentration of the electron shuttles on the electrode surface for a fast reaction of IET [5,6]. In this case, an electrode that possesses both nanopores and macroscopic pores could be most suitable for fast interfacial electron transfer in BES devices. Although lots of reports have revealed that hierarchical porous electrodes such as graphene aerogel-based materials, [7–9] natural biomass-derived porous materials [10–12] usually deliver excellent power generation performance in MFCs, the detailed mechanism for the porous structure affecting the DET and IET is not very clear.

For some electroactive microbes like *Shewanella* sp., DET and IET pathways actually take functions simultaneously when they utilize electrodes as electron acceptors [13,14]. Recently, it has been reported that the DET and IET processes can be clearly observed on the differential potential voltammograms of the carbon cloth anode [15,16]. However, these typical redox peaks are not always observable on the porous electrode, especially for DET peaks. It is possible that the interfacial electron transfer pathway is also dependent on the electrode structures. Since the IET and DET could be promoted via different electrode structures, it is possible to understand the mechanism via tailoring the nanopores and macroscopic pores of the electrode.

Carbon fiber electrodes are widely used macroscopic porous electrodes in MFCs. In recent years, the electrospinning technique was widely used as a versatile fabrication approach to produce nano-fibrillary materials applied in the fields of energy, electronics, biomedicine, etc. [17–20]. With this technology, it is possible to obtain carbon nanofibers with different fiber interspace via tailoring the fiber diameter and density. Further, with the introduction of the nano-structured templates into the electrospun precursors, fibers with internal pores or hollow structures could be obtained after the removal of the templates [21]. In this case, nanoporous carbon fiber nonwoven mats with controllable pore structures could be obtained via the electrospinning method. In this work, nanoporous carbon fiber (NPCF) nonwoven anode materials derived from electrospun polyacrylonitrile/zeolitic imidazolate framework-8 (PAN/ZIF-8) hybrid fibers have been developed for MFCs. The porous structure-dependent interfacial electron transfer behavior was investigated and a detailed mechanism was proposed based on the bioelectrocatalytic analysis of the NPCF electrodes and the biofilm morphology observation on the NPCF electrodes.

2. Results

2.1. Characterization of NPCFs

Before preparing the NPCF precursors, the size of nanoparticle templates was optimized to obtain uniform porous fibers. Three kinds of ZIF-8 nanoparticles with different diameters were prepared (Figure S1) and commercial ZnO nanoparticles with a diameter of 50 nm were also used as control. From the morphology of the hybrid fibers, only the one containing 50 nm ZIF-8 (Figure S2a–g) possesses uniform fiber diameter and even distribution of nanoparticles. For the 50 nm ZnO nanoparticles (Figure S2d,h) embedded fibers, it exhibits a necklace-like structure due to the aggregation of ZnO. It is possible that the organic frame structure of the ZIF-8 nanoparticles promotes their homogeneous distribution in the PAN precursors. In this case, the hybrid fibers containing 50 nm ZIF-8 nanoparticles were used as precursors for the following investigations. After the pyrolysis process at 900 °C and acid washing, three NPCFs with different ZIF-8:PAN weight ratios (0.5:1, 1:1, 2:1) in precursors have been obtained, which are shown in Figure 1 and Figure S3. In contrast to the carbonized PAN (CPAN) fibers, the NPCFs possess a larger fiber diameter and rougher surface with homogenous internal mesopores. It is also noted that with the increase of ZIF-8 amount in the precursors, the fiber diameter of the NPCFs increased from around 400 nm to about 1 μm. The high-resolution TEM images (Figure S4) reveal that the pore size (around 30–50 nm) is similar for the three NPCFs, while the increased ZIF-8 amount in the precursor certainly introduces more mesopores into the carbon fibers.

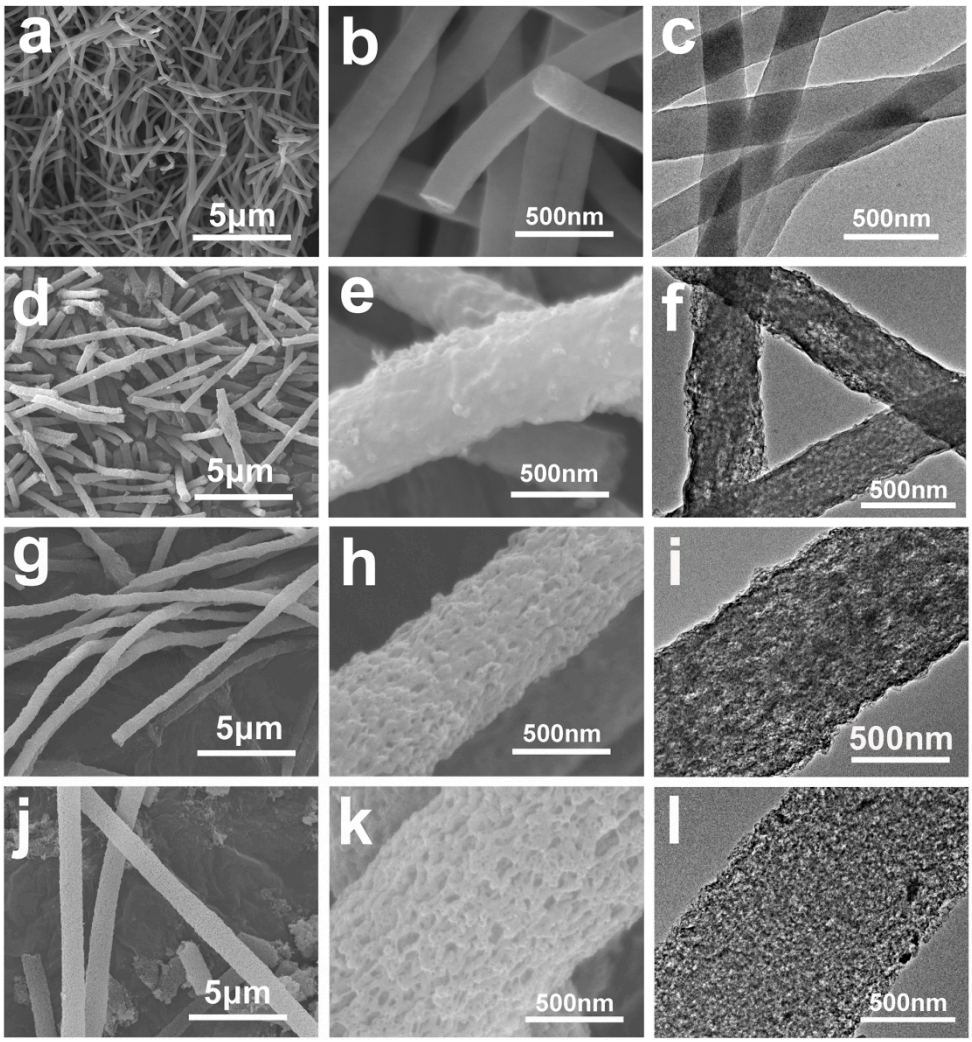

Figure 1. FESEM images (**a**,**b**,**d**,**e**,**g**,**h**,**j**,**k**) and TEM images of different carbon fibers. (**a**–**c**) CPAN, (**d**–**f**) NPCF-1, (**g**–**i**) NPCF-2, (**j**–**l**) NPCF-3.

To further explore the pore structure of different carbon fibers, they were examined with nitrogen adsorption-desorption analysis. The isotherms (Figure 2a) show that the NPCF-2 and NPCF-3 possess much higher pore volume than that of CPAN and NPCF-1 so the specific surface area of NPCF-2 (503 m^2 g^{-1}) and NPCF-3 (546 m^2 g^{-1}) are much higher than that of CPAN (7 m^2 g^{-1}) and NPCF-1 (47 m^2 g^{-1}) (Figure 2b). The pore size distribution based on the density functional theory (DFT) model (Figure 2c,d) indicates that the NPCF-3 possesses more mesopores (30–50 nm) and macropores (50–200) than the other two NPCFs. It is interesting that the NPCF-2 possesses more micropores than NPCF-3 so that it has a similar specific surface area to NPCF-3 although its total pore volume is less than that of NPCF-3.

For evaluation of the surface properties, crystal structures, and defects in different NPCFs, various physical characterizations including XPS, XRD, and Raman analyses were conducted. From XPS survey spectra (Figure S5), the NPCFs possess a lower nitrogen ratio but a higher oxygen ratio than that of CPAN, which is due to the introduction of the ZIF-8 nanoparticles in precursors. The XRD patterns (Figure S6a) show that all of the carbon fibers have the same crystal structure and the Raman spectra (Figure S6b) show that all of the samples possess a similar R ratio (ID/IG). These results suggest that the four carbon fiber materials possess similar defection structures. To evaluate the interspace between fibers, the apparent density of the three NPCF electrodes and the CPAN were also calculated (Table S1) [22–24]. The results indicate that as the fiber diameter increases, the apparent density of

carbon fibers is obviously decreased. It suggests that the fiber interspace increases with the fiber diameter increment while the fiber density (the number of fibers in a specific volume) is decreased with it. According to the above physical characterizations, the internal nanoporous structure as well as the fiber diameter related interspace of the NPCFs could be the dominant factors that determine the electrocatalytic performance of the NPCF anodes.

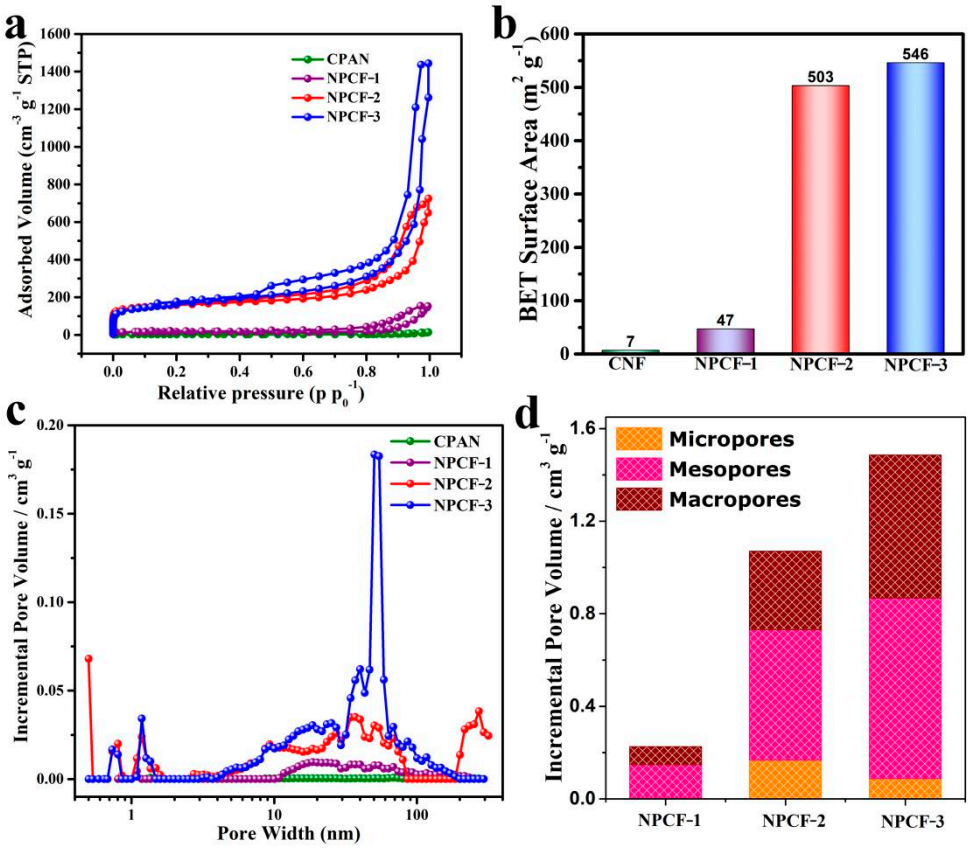

Figure 2. Nitrogen adsorption-desorption isotherms (**a**), BET surface area values (**b**) and DFT pore size distributions (**c**,**d**) of different NPCFs and CPAN.

2.2. Bioelectrocatalysis Behavior Analyses

The electrochemical behavior of different NPCF anodes was firstly investigated in flavin mononucleotide (FMN) solution to understand the interfacial redox reactions of flavin mediators on these porous carbon fibers. As shown in Figure 3a, all three NPCFs exhibit a good redox pair at around −0.45 V vs. SCE, which is attributed to the redox reaction of FMN. It is noted that the peak height values are proportional to the pore volume (especially to the volume of mesopores and macropores) rather than the specific surface area of the porous carbon fibers. The reason might be that the micropores are not suitable for FMN reaction 3 but contribute a lot to the specific surface area. In addition, the redox peaks increase continuously during the first 72 h in the FMN solution (Figure 3c), which suggests a slow adsorption process. To evaluate the adsorption behavior of different carbon fiber electrodes, a time-dependent oxidative peak variation profile (at an interval of 24 h) was investigated and recorded as shown in Figure 3d. For all electrodes, the redox peak reaches the maximum level at 72 h. After that, the anodes were transferred into the phosphate buffer without FMN, the decrease in the peak current could be observed due to the slow desorption of the FMN from the electrode surface. However, unlike the CPAN and NPCF-1, the NPCF-2 and NPCF-3 remain around 50% of peak height. It suggests that a large number of nanopores of these two carbon fiber electrodes promote the adsorption of FMN on the electrode surface and the adsorbed amount of FMN seems proportional to the pore volume. According to these results, the NPCF-2 and NPCF-3 electrodes could provide

higher concentrations of interfacial flavin mediators for the interfacial electron transfer between the bacteria and the electrode and may deliver much higher performance in the MFCs operation than the other two anodes.

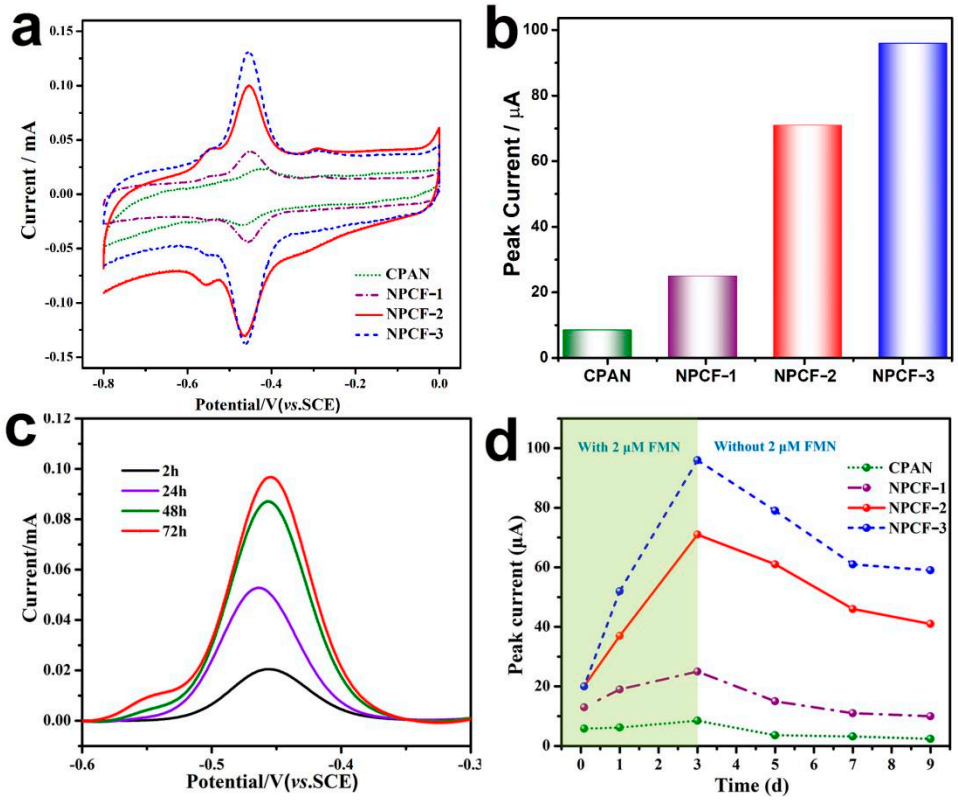

Figure 3. (**a**) CVs at the scan rate of 5 mv s^{-1} and (**b**) Peak current values of different carbon fiber electrodes in 0.1 M PBS buffer with 2 μM FMN, (**c**) the oxidative peak of NPCF-3 at a different time in 0.1 M PBS buffer with 2 μM FMN and subsequent transfer to 0.01 M PBS buffer, (**d**) time-dependent peak current variation of different carbon fiber electrodes.

To evaluate the bio-electrochemical catalysis performance of different carbon fiber anodes, they were applied in *S. putrefaciens* CN32-catalyzed MFCs with batch-type dual-chamber configuration. The power curves and the polarization curves are shown in Figure 4. It is noted that the NPCF-2 anode delivers a maximum power density of 997 mW m^{-2}, which is three-fold higher than that of the CPAN anode (277 mW m^{-2}) and ten-fold higher than that of the carbon cloth anode (101 mW m^{-2}, Table S1). Surprisingly, the NPCF-3 anode did not exhibit outstanding power output performance (903 mW m^{-2}) although it possesses the highest total pore volume and specific surface area. According to Figure 3a, the NPCF-2 anode possesses a higher double-layer capacitance current, which will significantly contribute to the power density [25,26]. That might be one reason for its superior performance in power output evaluation.

It is noted that the NPCF-1 anode also achieved a maximum power density of 829 mW m^{-2} although it possesses a much lower specific surface area and pore volume than that of NPCF-2 and NPCF-3. To explain this phenomenon, the electrocatalytic behavior of different anodes after biofilm formation (being poised at 0.2 V vs. SCE for 72 h) was investigated. The CVs with turnover current at the scan rate of 1 mV s^{-1} and DPV curves are shown in Figure 5. The starting potential of each catalytic wave on the turnover CVs is the same as the peak potential of DPVs. The DPVs show two peaks for all anodes. Besides the flavin oxidation peak at around −0.45 V, the broad peak at around 0–0.1 V could be attributed to a direct interfacial electron transfer occurring through a contact of the anode with a cytochrome independent of flavin.15 These results prove that the interfacial electron transfer process for each anode contains both flavin-mediated IET and

cytochromes-mediated DET. Interestingly, the proportion of IET and DET in the interfacial electron transfer is quite different for each anode. For the CPAN anode, the DET current is higher than that of the IET current while for NPCF-1, the IET current is a little bit higher than that of the DET current. The reason is that the internal nanopores greatly promoted the flavin-based IET. For NPCF-2 and NPCF-3 anodes, the IET peak is much higher than that of DET. From the overlaid DPV curves (Figure S7), the IET peaks variation profile for different anodes is similar to the behavior in the FMN solution. While for DET, the NPCF-1 has the highest peak while the NPCF-3 has the lowest one. It has been reported that the pore size of a few microns does not favor the efficient development of electroactive biofilms [27]. In this case, it is possible that the weak DET current on NPCF-3 might be due to the fact that the wider fibers with large interspace could not provide a suitable place for biofilm formation.

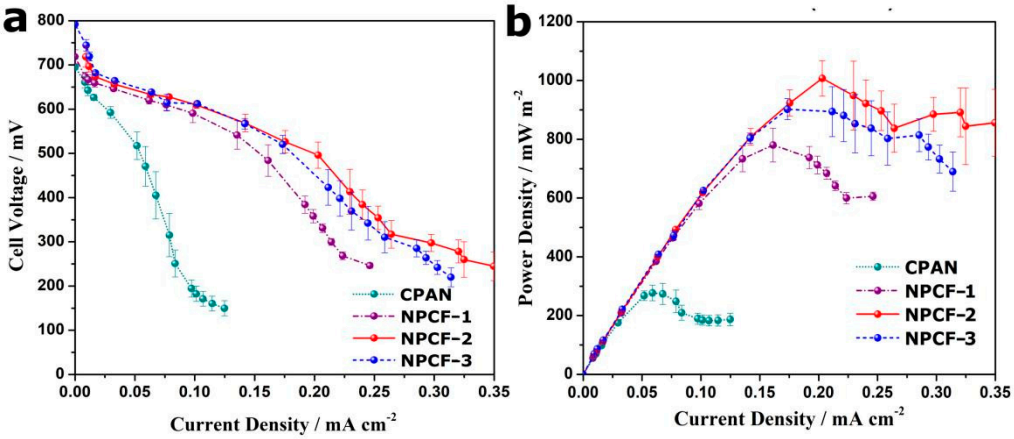

Figure 4. Polarization curves (**a**) and power curves (**b**) of different MFCs with five repeats.

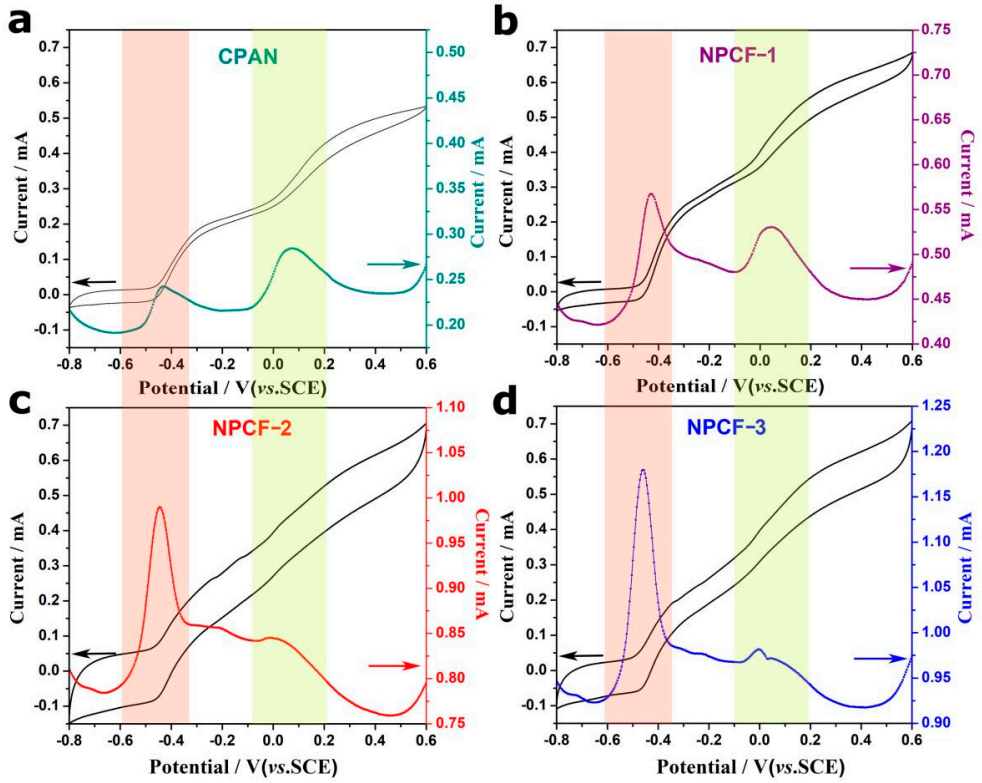

Figure 5. DPV and turnover CV curves of different porous carbon fiber anodes ((**a**): CPAN, (**b**): NPCF-1, (**c**): NPCF-2, (**d**): NPCF-3) in *S. putrefaciens* CN32 half-cells.

2.3. Biofilm Observation

To evaluate the biofilm formation on different anodes, the morphology of biofilm on anodes was examined by FESEM (Figure 6). As revealed in Figure 6, the NPCF anodes apparently promote bacteria adhesion, which is also proved by the protein analysis results (Figure S8). It is noted that the tightly adhered biofilm with extracellular polymeric substances (EPS) can be clearly observed on NPCF-1 and NPCF-2 anodes, and they have similar biofilm loading amounts. It has been reported that the EPS in the biofilm plays a key role in the extracellular electron transfer of Shewanella sp. cells [28]. For NPCF-3, the bacteria cells aggregate in the interspaces between the fibers, and the EPS structure is hard to observe. However, the total protein amount of NPCF-3 is higher than that of NPCF-1 and NPCF-2. The reason might be that the biofilm just covers the electrode but is not tightly adhered to the carbon fibers (Figure S9), In this case, this kind of biofilm may not contribute to the DET process. This might be the reason for the poor DET on the NPCF-3 anode.

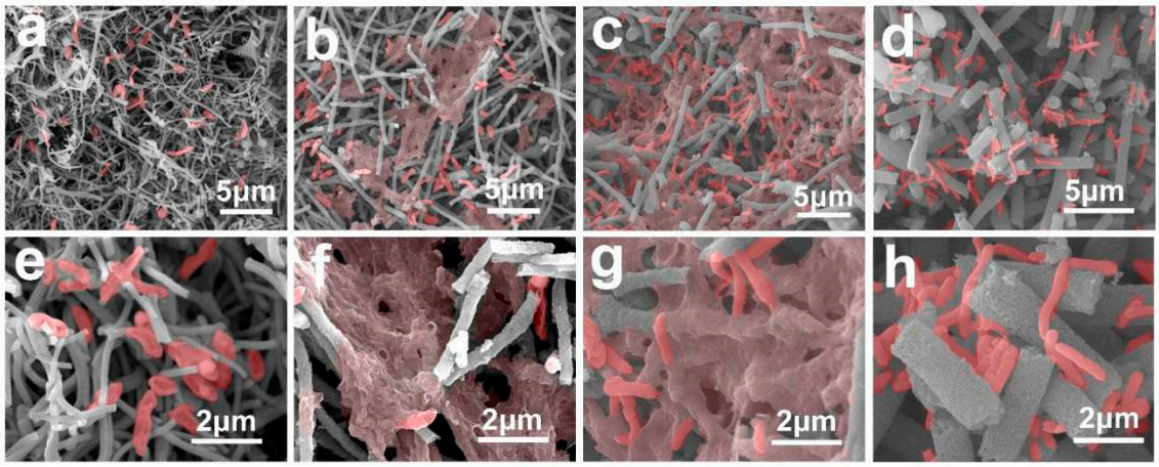

Figure 6. FESEM images of the bacterial cells adhered to the electrode surface after 14 days MFCs operation. (**a**,**e**) CPAN, (**b**,**f**) NPCF-1, (**c**,**g**) NPCF-2 and (**d**,**h**) NPCF-3.

2.4. Nanoporous Fiber Dependent Interfacial Electron Transfer Mechanism

According to the above discussions, the fiber diameter and internal nanoporous dependant interfacial electron transfer behavior between the nanoporous carbon fiber anode and the *S. putrefaciens* CN32 cells could be summarized in Figure 7. For the thinner fibers without internal nanopores (a), the DET could be achieved but the bacteria cell loading amount is not enough to achieve a high catalytic current. Further, they cannot provide enough surface for fast IET due to the lack of porous structure. For the carbon fiber anode with appropriate fiber diameter and internal nanopores (b), the bacteria cells can form a continuous biofilm with EPS structure on the fiber surface for DET. Beneath the biofilm, the mesopores promote the adsorption of the flavins and provide a large active surface area for fast IET. As a result, this kind of mesoporous carbon fiber anode could achieve superior power generation performance via an outstanding interfacial electron transfer process. For the quite thick mesoporous carbon fiber anode (c), the large interspace impedes the formation of tightly adhered continuous biofilm so that the DET process is limited. According to this mechanism, it is important to control the fiber diameter and the interspace besides the mesopores tailoring when designing the porous fiber electrode for optimal bioelectrocatalysis.

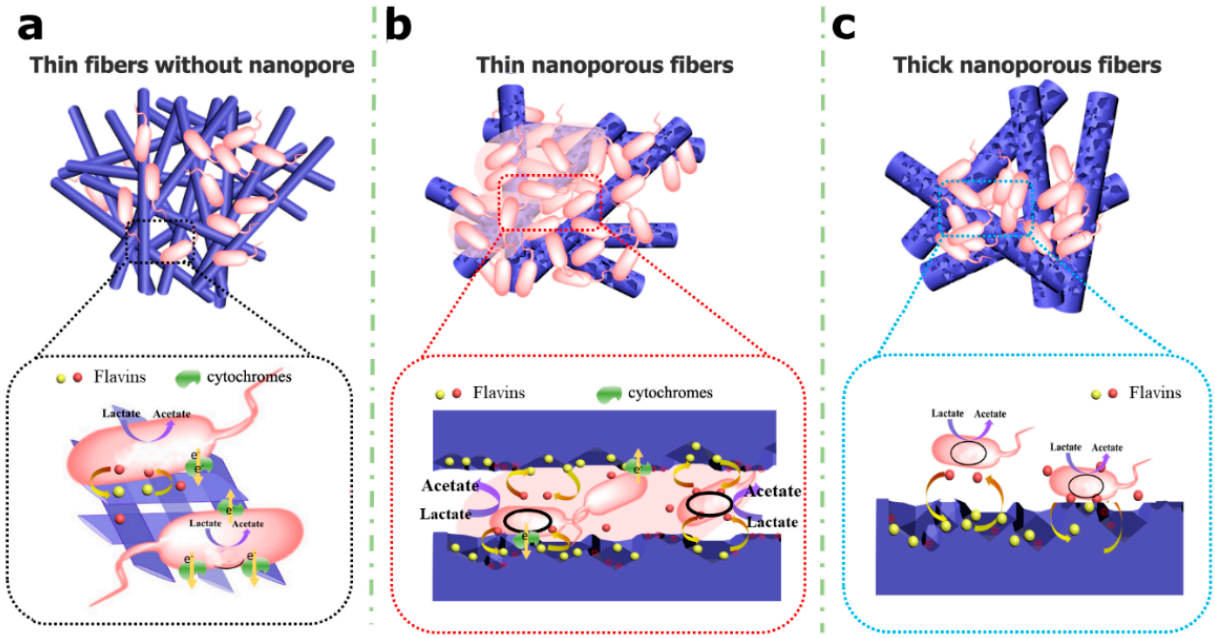

Figure 7. Proposed mechanism for structure-dependent interfacial electron transfer on nanoporous carbon fiber electrodes. (**a**) thin fibers without nanopores; (**b**) thin nanoporous fibers; (**c**) thick nanoporous fibers).

3. Materials and Methods

3.1. Preparation of ZIF-8 Particles

Firstly, 5.74 g of 2-methylimidazole (MeIM) was dissolved in 100 mL of ethanol. Then, 1.782 g $Zn(NO_3)_2 \cdot 6H_2O$ in 100 mL of ethanol was added to the above solution with magnetic stirring at room temperature for a few seconds. When the solution turns white, it was kept still at room temperature for 24 h. Next, the white powder was collected by centrifugation at 10,000 rpm for 5 min, washed thoroughly with ethanol three times, and dried at 60 °C for 12 h.

3.2. Preparation of Mesoporous Carbon Fibers

According to methods previously reported [29,30], different amounts of ZIF-8 (0.0875, 0.175, and 0.35 g) nanoparticles were added into 2.185 mL N, N-dimethylformamide (DMF) with sonication until it was well dispersed. Then, 0.175 g of ground polyacrylonitrile (PAN) powder was added to the former solution with stirring for around 30 h to form a homogeneously dispersed spinning solution. A 5 mL syringe capped with a flat metallic needle was filled with the spinning solution and mounted on an automatic syringe pump (Pump 11 Elite, Harvard, Holliston, MA, USA). The fibers were obtained by electrospinning with a positive voltage of 20 KV, a collecting distance of 18 cm, and an injection speed of 1.0 mL h^{-1} at 28 °C. After peroxidation at 280 °C for 2 h with a ramp rate of 1 °C min^{-1}, the fibers were carbonized under the protection of high purity argon gas through a two-stage heating process. In particular, the materials were carbonized at 550 °C for 1 h with a ramping rate of 2 °C min^{-1}, followed by a further pyrolysis process at 900 °C for 2 h with a ramping rate of 5 °C min^{-1}. The resultant composite nanofibers were soaked in sulfuric acid (3 M) under magnetic stirring for 3 h at room temperature, washed with ethanol, and deionized water several times. The final product was obtained by freeze-drying and stored under ambient conditions for the following experiments. The products synthesized with 0.0875, 0.175 and 0.35 g ZIF-8 were denoted as NPCF-1, NPCF-2 and NPCF-3, respectively. CPAN fibers synthesized without ZIF-8 were also treated with the same procedures as described above.

3.3. Bacterial Culture

A single clone of *S. putrefaciens* CN32 (ATCC® BBA-1097TM, ATCC, Manassas, VA, USA) was inoculated in 100 mL of Luriae Bertani (LB) broth medium (a mixture of 10 g L^{-1} sodium chloride, 10 g L^{-1} tryptone, 5 g L^{-1} yeast extract) overnight, and then 15 mL of bacterial culture suspension was inoculated in 200 mL of fresh LB broth and cultivated at 30 °C until the optical density at 600 nm (OD600) reached about 1.5. The cell pellets were further harvested by centrifugation at 4 °C (6000 rpm, 5 min), and then resuspended in 100 mL M9 buffer (Na_2HPO_4, 6 g L^{-1}, KH_2PO_4, 3 g L^{-1}, NaCl, 0.5 g L^{-1}, NH_4Cl, 1 g L^{-1}, $MgSO_4$, 1 mM, $CaCl_2$, 0.1 mM), which supplemented with 18 mM lactate as an electron donor. The resulting cell suspension was transferred into the anodic chamber of the MFC and purged with nitrogen gas for 0.5 h to remove the dissolved oxygen before the test.

3.4. Material Characterization

The morphologies of carbon fibers and biofilm-covered anodes were investigated by field emission scanning electron microscope (FESEM, JEOL, JSM-7800F, Tokyo, Japan). Transmission electron microscope 9TEM, JEOL, JEM-2100F, Tokyo, Japan) was also used for high-resolution observation of NPCFs. Before morphology observation, the biofilm-covered anodes were immersed in 4% polyoxymethylene for more than 12 h, then dehydrated with ethanol (30%, 40%, 50%, 60%, 70%, 80%, 90%, and 100%) and dried in vacuum at room temperature overnight. X-ray photoelectron spectroscopy (XPS) spectrums were performed on an X-ray photoelectron spectrometer (Thermo Fisher Scientific Inc, ESCALAB 250Xi, Waltham, MA, USA). Power X-ray diffraction (XRD) patterns were recorded on an X-ray diffractometer (XRD-7000, Shimadzu, Tokyo, Japan) at 40 kV and 30 mA with Cu Kα radiation (λ = 0.15406 nm) in the step of 2° min^{-1} and a 2θ range from 10° to 80°. N2 adsorption-desorption analysis was measured on an ASAP 2020 (Micromeritics, Norcross, GA, USA) accelerated surface area and porosimetry system at 77 K using Barrett-Emmett-Teller (BET) calculations for the surface area. The pore size distribution plot was conducted with the desorption branch of the isotherm on the density functional theory (DFT) model ranging from micropores to macropores. DFT model could describe adsorption over the entire range of carbon pore sizes and accurately describe the density profile of the inhomogeneous adsorbed nitrogen within carbon slit pores [31].

3.5. MFC Set Up and Operation

The H-shaped dual-chamber MFC device consisting of two 100 mL glass flasks (Figure S10) separated by a proton exchange membrane (PEM, Nafion 117, Dupont, Wilmington, DE) was used in this work. The NPCF material (3 mg cm^{-2}) coated on carbon cloth was used as the MFC anode, and a carbon fiber brush as a cathode. The catholyte was 0.01 M phosphate buffer with 50 mM potassium ferricyanide. The MFCs with 1.5 kΩ constant load resistance were running at 30 °C with a digital multimeter recording the output voltage. The polarization and power curves were investigated by varying the external load resistor from 1 kΩ to 80 kΩ to obtain a stable current.

3.6. Electrochemical Analysis

All the cyclic voltammetry (CV) and differential pulse voltammetry (DPV) experiments were carried out with CHI 660E electrochemical working station (CHI Instrument, Shanghai, China) in a three-electrode electrochemical cell including the working electrode, a saturated calomel electrode (SCE) as reference electrode and a titanium plate as a counter electrode. All potentials reported in this work are presented versus SCE.

4. Conclusions

In summary, nanoporous carbon fiber electrodes were successfully fabricated through a facile electrospinning-pyrolysis process. In comparison to the CPAN and carbon cloth electrodes, all three nanoporous carbon fiber electrodes exhibited superior bioelectrocatalytic performance according to their specific porous structure. The mesopores improved

the kinetic process of flavin-based interfacial redox reaction and promoted the adsorption of flavins to guarantee fast IET. Meanwhile, the interspace between the electrospun fibers will affect the biofilm formation as well as the DET process. The continuous biofilm with EPS will transform into dispersed cell aggregates when the diameter of carbon fibers, as well as the interspaces, are increasing. According to the findings of this work, both the mesoporous structure and the fiber interspaces should be concerned when designing porous fiber electrodes in MFCs or other bioelectrochemical system devices. Considering the facile process and relatively low cost, the electrospun mesoporous fiber-derived carbon fiber electrode could be a promising candidate for high-performance, large-scale MFCs or even other bioelectrochemical systems.

Supplementary Materials: The following supporting information can be downloaded at: https://www.mdpi.com/article/10.3390/catal12101187/s1, Figure S1: FESEM images of ZIF-8 nanoparticles of different sizes (a) 50 nm, (b) 100 nm and (c) 200 nm, Figure S2: FESEM images of electrospun carbon fibers prepared by different nano templates. (a,d) ZnO nanoparticles of 50nm, (b,e) ZIF-8 nanoparticles of 100nm, (c,f) ZIF-8 nanoparticles of 200 nm, Figure S3: FESEM images of cross-section of carbon fibers (a) CPAN, (b) NPCF-1, (c) NPCF-2, (d) NPCF-3, Figure S4: TEM images of carbon fibers (a) CPAN, (b) NPCF-1, (c) NPCF-2, (d) NPCF-3, Figure S5: (a) XPS survey spectra, (b) the atomic percentage of N and O of CPAN, NPCF-1, NPCF-2 and NPCF-3, Figure S6: Raman spectra and XRD patterns of CPAN, NPCF-1, NPCF-2 and NPCF-3, Figure S7: DPV curves of different anodes in the, Figure S8: Total protein content of the biofilm on CPAN, NPCF-1, NPCF-2 and NPCF-3, Figure S9: (a) The biofilm covered on NPCF-3 anode; (b) morphology of the area without biofilm coverage for NPCF-3 anode, Figure S10: Dual-chamber MFC device, Table S1: Summary of the diameter, bulk density, ID/IG ratio and power density of different carbon fiber materials.

Author Contributions: Conceptualization, R.W. and Y.Q.; methodology, R.W., X.W., C.L., J.Y. and X.L.; validation, L.Z. and X.W.; formal analysis, R.W., X.W., C.L. and J.Y; investigation, R.W.; data curation, R.W. and X.L.; writing—original draft preparation, R.W.; writing—review and editing, Y.Q. and Z.L.; visualization, X.W.; supervision, Z.L. and Y.Q.; project administration, Y.Q.; funding acquisition, Y.Q. and L.Z. All authors have read and agreed to the published version of the manuscript.

Funding: This research was funded by Chongqing Key Laboratory for Advanced Materials and Technologies of Clean Energies, the Natural Science Foundation of Jiangxi Province (No. 20202ACB215001).

Conflicts of Interest: The authors declare no conflict of interest.

References

1. Kumar, A.; Hsu, L.H.-H.; Kavanagh, P.; Barrière, F.; Lens, P.N.L.; Lapinsonnière, L.; Lienhard V, J.H.; Schröder, U.; Jiang, X.; Leech, D. The ins and outs of microorganism–electrode electron transfer reactions. *Nat. Rev. Chem.* **2017**, *1*, 0024. [CrossRef]
2. Brutinel, E.D.; Gralnick, J.A. Shuttling happens: Soluble flavin mediators of extracellular electron transfer in Shewanella. *Appl. Microbiol. Biotechnol.* **2011**, *93*, 41–48. [CrossRef] [PubMed]
3. Zou, L.; Qiao, Y.; Wu, Z.-Y.; Wu, X.-S.; Xie, J.-L.; Yu, S.-H.; Guo, J.; Li, C.M. Tailoring Unique Mesopores of Hierarchically Porous Structures for Fast Direct Electrochemistry in Microbial Fuel Cells. *Adv. Energy Mater.* **2015**, *6*, 1501535. [CrossRef]
4. Tang, W.; Wu, X.-S.; Qiao, Y.; Wang, R.-J.; Luo, X. Tailoring of pore structure in mesoporous carbon for favourable flavin mediated interfacial electron transfer in microbial fuel cells. *RSC Adv.* **2018**, *8*, 9597–9602. [CrossRef] [PubMed]
5. Qiao, Y.; Qiao, Y.-J.; Zou, L.; Ma, C.-X.; Liu, J.-H. Real-time monitoring of phenazines excretion in Pseudomonas aeruginosa microbial fuel cell anode using cavity microelectrodes. *Bioresour. Technol.* **2015**, *198*, 1–6. [CrossRef]
6. Qiao, Y.-J.; Qiao, Y.; Zou, L.; Wu, X.-S.; Liu, J.-H. Biofilm promoted current generation of Pseudomonas aeruginosa microbial fuel cell via improving the interfacial redox reaction of phenazines. *Bioelectrochemistry* **2017**, *117*, 34–39. [CrossRef]
7. Yong, Y.-C.; Dong, X.-C.; Chan-Park, M.B.; Song, H.; Chen, P. Macroporous and Monolithic Anode Based on Polyaniline Hybridized Three-Dimensional Graphene for High-Performance Microbial Fuel Cells. *ACS Nano* **2012**, *6*, 2394–2400. [CrossRef] [PubMed]
8. Yong, Y.-C.; Yu, Y.-Y.; Zhang, X.; Song, H. Highly Active Bidirectional Electron Transfer by a Self-Assembled Electroactive Reduced-Graphene-Oxide-Hybridized Biofilm. *Angew. Chem. Int. Ed.* **2014**, *53*, 4480–4483. [CrossRef]
9. Zou, L.; Huang, Y.; Wu, X.; Long, Z.-E. Synergistically promoting microbial biofilm growth and interfacial bioelectrocatalysis by molybdenum carbide nanoparticles functionalized graphene anode for bioelectricity production. *J. Power Sources* **2018**, *413*, 174–181. [CrossRef]
10. Zhu, H.; Wang, H.; Li, Y.; Bao, W.; Fang, Z.; Preston, C.; Vaaland, O.; Ren, Z.; Hu, L. Lightweight, conductive hollow fibers from nature as sustainable electrode materials for microbial energy harvesting. *Nano Energy* **2014**, *10*, 268–276. [CrossRef]

11. Singh, S.; Bairagi, P.K.; Verma, N. Candle soot-derived carbon nanoparticles: An inexpensive and efficient electrode for microbial fuel cells. *Electrochim. Acta* **2018**, *264*, 119–127. [CrossRef]
12. Wu, X.; Qian, Y.; Shi, Z.; Li, C. Enhancement of interfacial bioelectrocatalysis in Shewanella microbial fuel cells by a hierarchical porous carbon–silica composite derived from distiller's grains. *Sustain. Energ. Fuels* **2018**, *2*, 655–662. [CrossRef]
13. Xiao, X.; Xia, H.-Q.; Wu, R.; Bai, L.; Yan, L.; Magner, E.; Cosnier, S.; Lojou, E.; Zhu, Z.; Liu, A. Tackling the Challenges of Enzymatic (Bio)Fuel Cells. *Chem. Rev.* **2019**, *119*, 9509–9558. [CrossRef]
14. Zou, L.; Qiao, Y.; Zhong, C.; Li, C.M. Enabling fast electron transfer through both bacterial outer-membrane redox centers and endogenous electron mediators by polyaniline hybridized large-mesoporous carbon anode for high-performance microbial fuel cells. *Electrochim. Acta* **2017**, *229*, 31–38. [CrossRef]
15. Choi, S.; Kim, B.; Chang, I.S. Tracking of Shewanella oneidensis MR-1 biofilm formation of a microbial electrochemical system via differential pulse voltammetry. *Bioresour. Technol.* **2018**, *254*, 357–361. [CrossRef] [PubMed]
16. Hassan, S.H.; Kim, Y.S.; Oh, S.-E. Power generation from cellulose using mixed and pure cultures of cellulose-degrading bacteria in a microbial fuel cell. *Enzym. Microb. Technol.* **2012**, *51*, 269–273. [CrossRef]
17. Manickam, S.S.; Karra, U.; Huang, L.; Bui, N.-N.; Li, B.; McCutcheon, J.R. Activated carbon nanofiber anodes for microbial fuel cells. *Carbon* **2013**, *53*, 19–28. [CrossRef]
18. Li, X.; Chen, Y.; Huang, H.; Mai, Y.W.; Zhou, L. Electrospun carbon-based nanostructured electrodes for advanced energy storage—A review. *Energy Storage Mater.* **2016**, *5*, 58–92. [CrossRef]
19. Chen, S.; Hou, H.; Harnisch, F.; Patil, S.A.; Carmona-Martinez, A.A.; Agarwal, S.; Zhang, Y.; Sinha-Ray, S.; Yarin, A.L.; Greiner, A.; et al. Electrospun and solution blown three-dimensional carbon fiber nonwovens for application as electrodes in microbial fuel cells. *Energy Environ. Sci.* **2011**, *4*, 1417–1421. [CrossRef]
20. Lu, X.; Wang, C.; Favier, F.; Pinna, N. Electrospun Nanomaterials for Supercapacitor Electrodes: Designed Architectures and Electrochemical Performance. *Adv. Energy Mater.* **2016**, *7*. [CrossRef]
21. Zhang, L.; Zeng, Y.; Cheng, Z. Removal of heavy metal ions using chitosan and modified chitosan: A review. *J. Mol. Liq.* **2016**, *214*, 175–191. [CrossRef]
22. Hao, P.; Zhao, Z.; Tian, J.; Li, H.; Sang, Y.; Yu, G.; Cai, H.; Liu, H.; Wong, C.P.; Umar, A. Hierarchical porous carbon aerogel derived from bagasse for high performance supercapacitor electrode. *Nanoscale* **2014**, *6*, 12120–12129. [CrossRef] [PubMed]
23. Lee, D.; Jung, J.-Y.; Jung, M.-J.; Lee, Y.-S. Hierarchical porous carbon fibers prepared using a SiO2 template for high-performance EDLCs. *Chem. Eng. J.* **2015**, *263*, 62–70. [CrossRef]
24. Zhu, X.; Cui, W.; Li, X.; Jin, Y. Electrospun Fibrous Mats with High Porosity as Potential Scaffolds for Skin Tissue Engineering. *Biomacromolecules* **2008**, *9*, 1795–1801. [CrossRef]
25. Feng, C.; Lv, Z.; Yang, X.; Wei, C. Anode modification with capacitive materials for a microbial fuel cell: An increase in transient power or stationary power. *Phys. Chem. Chem. Phys.* **2014**, *16*, 10464–10472. [CrossRef] [PubMed]
26. He, G.; Gu, Y.; He, S.; Schroder, U.; Chen, S.; Hou, H. Effect of fiber diameter on the behavior of biofilm and anodic performance of fiber electrodes in microbial fuel cells. *Bioresour. Technol.* **2011**, *102*, 10763–10766. [CrossRef] [PubMed]
27. Chong, P.; Erable, B.; Bergel, A. Effect of pore size on the current produced by 3-dimensional porous microbial anodes: A critical review. *Bioresour. Technol.* **2019**, *289*, 121641. [CrossRef]
28. Xiao, Y.; Zhang, E.; Zhang, J.; Dai, Y.; Yang, Z.; Christensen, H.E.M.; Ulstrup, J.; Zhao, F. Extracellular polymeric substances are transient media for microbial extracellular electron transfer. *Sci. Adv.* **2017**, *3*, e1700623. [CrossRef]
29. Chen, L.-F.; Lu, Y.; Yu, L.; Lou, X.W. Designed formation of hollow particle-based nitrogen-doped carbon nanofibers for high-performance supercapacitors. *Energy Environ. Sci.* **2017**, *10*, 1777–1783. [CrossRef]
30. Yao, Y.; Wu, H.; Huang, L.; Li, X.; Yu, L.; Zeng, S.; Zeng, X.; Yang, J.; Zou, J. Nitrogen-enriched hierarchically porous carbon nanofiber network as a binder-free electrode for high-performance supercapacitors. *Electrochim. Acta* **2017**, *246*, 606–614. [CrossRef]
31. Qiao, Y.; Wu, X.-S.; Li, C.M. Interfacial electron transfer of Shewanella putrefaciens enhanced by nanoflaky nickel oxide array in microbial fuel cells. *J. Power Sources* **2014**, *266*, 226–231. [CrossRef]